Contribution of Atmospheric Oxygenated Organic Compounds to Particle Growth in an Urban Environment

Qiao, Xiaohui

2021-10-19

Qiao , X , Yan , C , Li , X , Guo , Y , Yin , R , Deng , C , Li , C , Nie , W , Wang , M , Cai , R , Huang , D , Wang , Z , Yao , L , Worsnop , D R , Bianchi , F , Liu , Y , Donahue , N M , Kulmala , M & Jiang , J 2021 , ' Contribution of Atmospheric Oxygenated Organic Compounds to Particle Growth in an Urban Environment ' , Environmental Science & Technology , vol. 55 , no. 20 , pp. 13646-13656 . https://doi.org/10.1021/acs.est.1c02095

http://hdl.handle.net/10138/341154
https://doi.org/10.1021/acs.est.1c02095

submittedVersion

Contribution of atmospheric oxygenated organic compounds to particle growth in an urban environment

Journal:	*Environmental Science & Technology*
Manuscript ID	es-2021-02095k.R2
Manuscript Type:	Article
Date Submitted by the Author:	14-Aug-2021
Complete List of Authors:	Qiao, Xiaohui; Tsinghua University, School of Environment Yan, Chao; University of Helsinki, Institute for Atmospheric and Earth System Research INAR / Physics Li, Xiaoxiao; Tsinghua University, School of Environment Guo, Yishuo; Beijing University of Chemical Technology, Beijing Advanced Innovation center for Soft Matter Science and Engineering Yin, Rujing; Tsinghua University Deng, Chenjuan; Tsinghua University, School of Environment Li, Chang; Beijing University of Chemical Technology, Beijing Advanced Innovation center for Soft Matter Science and Engineering Nie, Wei; Nanjing University, School of Atmospheric Sciences Wang, MingYi; Carnegie Mellon University, Chemistry Cai, Runlong; University of Helsinki, Faculty of Science Huang, Dan Dan; Shanghai Academy of Environmental Sciences, CBME Wang, Zhe; The Hong Kong University of Science and Technology, Division of Environment and Sustainability Yao, Lei; University of Helsinki, Institute for Atmospheric and Earth System Research INAR / Physics Worsnop, Douglas; Aerodyne Research Inc, Bianchi, Federico; University of Helsinki, Institute for Atmospheric and Earth System Research INAR / Physics Liu, Yongchun; Beijing University of Chemical Technology, Beijing Advanced Innovation center for Soft Matter Science and Engineering Donahue, Neil M.; Carnegie Mellon University, Chemistry Kulmala, Markku; Helsingin Yliopisto, Dept. of Physical Sciences Jiang, Jingkun; Tsinghua University, School of Environment

Contribution of atmospheric oxygenated organic compounds to particle growth in an urban environment

Xiaohui Qiao[1], Chao Yan[2,3,], Xiaoxiao Li[1], YiShuo Guo[3], Rujing Yin[1], Chenjuan Deng[1], Chang Li[3], Wei Nie[4], Mingyi Wang[5], Runlong Cai[2,3], Dandan Huang[7], Zhe Wang[8], Lei Yao[2], Douglas R. Worsnop[2,9], Federico Bianchi[2,3], Yongchun Liu[3], Neil M. Donahue[5,6], Markku Kulmala[2,3], Jingkun Jiang[1,*]*

[1] State Key Joint Laboratory of Environment Simulation and Pollution Control, School of Environment, Tsinghua University, 100084 Beijing

[2] Institute for Atmospheric and Earth System Research/Physics, Faculty of Science, University of Helsinki, 00014 Helsinki, Finland

[3] Aerosol and Haze Laboratory, Beijing Advanced Innovation Center for Soft Matter Science and Engineering, Beijing University of Chemical Technology, 100029 Beijing, China

[4] Joint International research Laboratory of Atmospheric and Earth System Research, School of Atmospheric Sciences, Nanjing University, Nanjing, China

[5] Center for Atmospheric Particle Studies, Carnegie Mellon University, Pittsburgh, PA, USA

[6] Department of Chemistry, Carnegie Mellon University, Pittsburgh, PA, USA

[7] State Environmental Protection Key Laboratory of Formation and Prevention of Urban Air Pollution Complex, Shanghai Academy of Environmental Sciences, Shanghai, China

[8] Division of Environment and Sustainability, The Hong Kong University of Science and Technology, Hong Kong SAR, China

[9] Aerodyne Research Inc., Billerica, Massachusetts 01821, USA

Abstract Graphic:

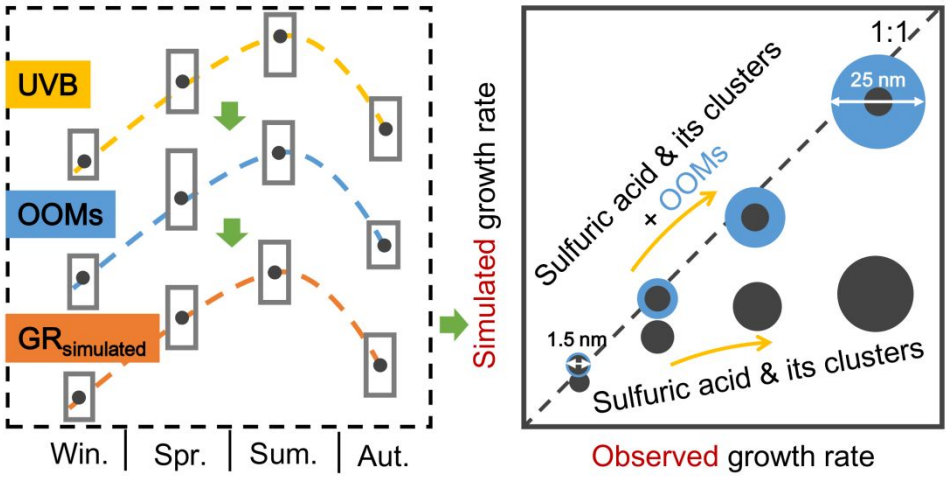

ABSTRACT. Gas-phase oxygenated organic molecules (OOMs) can contribute substantially to the growth of newly formed particles. However, the characteristics of OOMs and their contributions to particle growth rate are not well understood in urban area, which has complex anthropogenic emissions and atmospheric conditions. We performed long-term measurement of gas-phase OOMs in urban Beijing during 2018-2019 using nitrate-based chemical ionization mass spectrometry. OOM concentrations showed clear seasonal variations, with the highest in summer and the lowest in winter. Correspondingly, calculated particle growth rates due to OOM condensation were highest in summer, followed by spring, autumn, and winter. One prominent feature of OOMs in this urban environment was a high fraction (~75%) of nitrogen-containing OOMs. These nitrogen-containing OOMs contributed only 50%-60% of the total growth rate led by OOM condensation, owing to their slightly higher volatility than non-nitrate OOMs. By comparing the calculated condensation growth rates and the observed particle growth rates, we showed that sulfuric acid and its clusters are the main contributors to the growth of sub-3 nm particles, with OOMs significantly promoting the growth of 3-25 nm particles. In winter Beijing, there are missing contributors to the growth of particles above 3 nm, which remain to be further investigated.

KEYWORDS. Oxygenated Organic Molecules, Seasonal Variation, Particle Growth, Nitrogen-containing OOMs, Urban Environment

SYNOPSIS. Atmospheric oxygenated organic molecules with clear seasonal variations contribute significantly to the growth of newly formed nanoparticles in urban Beijing.

1 Introduction

Atmospheric new particle formation (NPF) happens ubiquitously in various environments, and particles growing past a size of around 50 nm can be activated as the cloud condensation nuclei (CCN), which influence cloud formation and climate.[1-3] NPF in polluted environments, despite the severe suppression by high aerosol loadings, has been shown to produce a large number of nanoparticles; these particles, if they survive scavenging by large existing particles, can grow and act as CCN.[4-6] Therefore, as a crucial determining factor for particle survival, particle growth rate can substantially influence the CCN budget.[7]

Condensable vapors, such as sulfuric acid, are important contributors to the growth of particles in various environments due to their low volatility.[8-10] Observations in Atlanta indicated that condensation of sulfuric acid and the subsequent equilibration with ammonia could substantially account for nanoparticle growth.[11] Also, it has been illustrated recently that condensation of H_2SO_4 and H_2SO_4-amine clusters contribute significantly to the growth of sub-3 nm particles in urban Beijing; however, sulfuric acid and its clusters alone cannot explain the growth of particles above 3 nm.[10] This is still far from "climate-relevant" size. There are still some missing contributors to particle growth, especially beyond the earliest stages.

Gas-phase oxygenated organic molecules (OOMs) are important for particle growth and even largely explain the particle growth rate in forested areas owing to their low volatility.[12-14] OOMs can be produced from the oxidation of volatile organic compounds (VOCs), including anthropogenic volatile organic compounds (AVOCs, e.g., benzene and toluene) and biogenic volatile organic compounds (BVOCs, e.g., isoprene, monoterpenes, and sesquiterpenes).[15-18] Chamber experiments have shown that the oxidation products of monoterpenes alone can trigger particle formation and drive the following growth.[19-22] Consistently, ambient observations in a boreal forest in southern Finland (Hyytiälä) have shown that BVOC-derived OOMs are sufficient to explain particle growth over the size range of 3-50 nm.[13]

In contrast to remote forests, AVOCs are usually the dominant VOC species in urban environments, and NO_x levels are usually much higher. Thus the characteristics of OOMs in polluted urban environments might be substantially different from those in forested areas. For BVOCs, auto-oxidation of RO_2 radicals is an important pathway of OOM formation.[14, 18, 23] Each auto-oxidation step results in an addition of two oxygen atoms, which greatly increases the oxygen number of OOMs.[16, 24, 25] For AVOCs, multi-generation oxidation is also an important pathway in OOMs formation.[26] This is mainly because the abundant NO_x in urban areas can suppress the auto-oxidation and terminate the chain propagation,[27] but also because the oxidation lifetime of later-generation AVOC products can be much lower than the precursor AVOCs.[28] As a result, OOMs generated under high NO_x conditions may have relatively higher volatilities than those in low NO_x conditions.[26, 27, 29] In wintertime Beijing, Yan et al.[30] demonstrated that OOMs are important for particle growth to CCN size. In another study in summertime Beijing, Brean et al.[31] showed that elevated OOM concentrations and particle growth coincided, implying an important contribution

of OOMs to particle growth in urban areas. However, neither study had a quantitative evaluation of the contribution of OOMs to particle growth, and the contribution in different seasons has not been examined.

We conducted measurements of OOMs in urban Beijing during Jan. 2018 – Aug. 2019 covering four seasons. We investigated the overall characteristics of OOMs in urban Beijing in comparison to those in other atmospheric environments. We further evaluated the contribution of OOMs to particle growth over a size range of 1.5-25 nm and explored the dominant factors of its seasonal variation. Finally, we compared the calculated particle growth rates explained by sulfuric acid (include its clusters) and non-/nitrated OOMs to the observed values.

2 Methods

2.1 Measurements

The field measurements were conducted at an urban site located inside the west campus of Beijing University of Chemical Technology. The station is ~500 meters west to the Third Ring Road and is surrounded by residential and commercial areas. A detailed description about this site can be found in previous studies.[10, 32] The measurements were between Jan. 2018 and Aug. 2019, covering all the four seasons and including 27 NPF events with reliable OOMs and particle growth rate data in total. The exact duration of the four seasons are Mar. 3 – Apr. 7 2018 for spring with 5 NPF cases, Oct. 16 – Nov. 31 for autumn with 5 NPF cases, Jan. 25 – Feb. 6 and Dec. 10 – Dec. 24 2018 for winter with 11 NPF cases, and Jun. 15 – Aug. 31 2019 for summer with 6 NPF cases, respectively.

OOMs and H_2SO_4 were measured with nitrate-based chemical ionization atmospheric pressure interface time-of-flight mass spectrometers (CI-APi-ToF, Aerodyne Research Inc.).[33, 34] A high-resolution time-of-flight mass spectrometer with the m/z resolution of ~4000 Th/Th (CI-APi-HToF) was used in 2018, and a long time-of-flight mass spectrometer with the m/z resolution of ~10000 Th/Th (CI-APi-LToF) was used in 2019. Both instruments were calibrated for H_2SO_4 sensitivity and m/z-dependent transmission efficiency following previous studies.[20, 35] Details of the sampling configurations are similar with those previously described.[10] In addition, H_2SO_4 clusters in this study refer to clusters containing up to four H_2SO_4 molecules and some base

116 molecules as stabilizing agents. The concentration of these clusters was estimated using the
117 simplified kinetic model described in Cai et al.[36]

118 Particle number concentrations and size distributions ranging from 1 nm to 10 μm were measured
119 by a diethylene glycol scanning mobility particle spectrometer (DEG-SMPS; 1-7.5 nm)[37, 38]
120 together with a particle size distribution system (PSD; 3-10 μm).[39] A core sampling method was
121 used in the DEG-SMPS system to achieve an aerosol sampling efficiency close to 100%.[40] A
122 miniature cylindrical differential mobility analyzer (mini-cyDMA) was equipped for sub-10 nm
123 aerosol classification and a modified DEG-UCPC with two-stage temperature control chamber
124 was used for as the front equipment for particle counting.[41] Meteorological data, including
125 temperature, ambient pressure, wind speed, and wind direction, were measured with a local
126 weather station (Vaisala, AWS310).

127 **2.2 OOMs quantification**

128 OOM identification was performed with the tofTools package developed by Junninen et al.[42] The
129 low background noises of the CI-APi-ToF are automatically removed in software. After obtaining
130 the signals of assigned peaks, the concentrations of OOMs are calculated using Eq. 1:[20, 35]

$$[\mathrm{OOM_i}] = C \times T_i \times \ln\left(1 + \frac{[\mathrm{OOM_i} \cdot \mathrm{NO_3^-}]}{\sum_{i=0}^{2}[(\mathrm{HNO_3})_i \cdot \mathrm{NO_3^-}]}\right) \qquad \text{Eq. (1)}$$

131 Here, OOM signals in counts per second $[\mathrm{OOM_i} \cdot \mathrm{NO_3^-}]$ are normalized to the sum of reagent ion
132 signals, including $\mathrm{NO_3^-}$, $(\mathrm{HNO_3})\mathrm{NO_3^-}$, and $(\mathrm{HNO_3})_2\mathrm{NO_3^-}$. T_i is the mass-dependent transmission
133 efficiency of the instrument, which was determined by adding different perfluorinated acid vapors
134 in sufficient amounts to deplete $\mathrm{NO_3^-}$.[35] C is the calibration coefficient obtained for H_2SO_4 using
135 a homemade H_2SO_4 generator.[43] We conducted four calibrations during the observation period.
136 The calibration coefficients are 4.79×10^9 and 4.5×10^9 $cm^{-3} \cdot cps^{-1}$ for CI-APi-HToF in 2018, 6.07
137 $\times 10^9$ and 6.47×10^9 $cm^{-3} \cdot cps^{-1}$ for CI-APi-LToF in 2019. Here, we assume OOMs and H_2SO_4
138 have the same collision and binding efficiency with $\mathrm{NO_3^-}$.[18] The charging efficiency for some less
139 functionalized OOMs is likely lower than that for H_2SO_4, and therefore, the total OOM
140 concentration measured by nitrate-based CI-APi-TOF should be regarded as a lower limit.

2.3 OOMs volatility estimation

Due to the lack of molecular structure information, OOM volatility was estimated using volatility parameterization methods based on the number of carbon, oxygen, and nitrogen atoms of the identified molecule.[44] As suggested by a recent study,[45] two volatility parameterization methods that treat OOMs with different functional groups were adopted in this study. One is for OOMs that mainly contain hydroperoxide groups, such as products via auto-oxidation:[13]

$$\log_{10} C^*_{300\,K} = (25 - n_C)b_C - (n_O - 3n_N)b_O - 2\frac{(n_O - 3n_N)n_C}{(n_C + n_O - 3n_N)}b_{CO} - n_N b_N \qquad \text{Eq. (2)}$$

where $b_C = 0.475$, $b_O = 0.2$, $b_{CO} = 0.9$, and $b_N = 2.5$, and n_C, n_O, and n_N are the number of carbon, oxygen, and nitrogen atoms in the compounds, respectively. The other is for OOMs that mainly contain hydroxyl and carboxylic groups, such as products via multi-generation oxidation:[45]

$$\log_{10} C^*_{300\,K} = (25 - n_C)b_C - (n_O - 2n_N)b_O \qquad \text{Eq. (3)}$$

where $b_C = 0.475$, and $b_O = 2.3$. A nitrate group reduces the similar extent of vapor pressure like a hydroxyl, and is replaced by hydroxyl for simplicity.[45] In terms of the oxidation pathway and the resulting functional groups, oxidation products of isoprene are also suitable for Eq. 3.[24] An empirical dividing line of H/C = -0.2*O/C + 1.5 is adopted in this study to separate OOMs with different kinds of main functional groups corresponding to the above two parameterization methods. The volatility of OOM above the line is estimated by Eq. 2, and otherwise by Eq. 3. More details about the volatility estimation method are in the supplemental information.

OOMs measured by nitrate CI-APi-ToF are partly extremely low or low volatility organic compounds in Beijing (Fig. S6). The over-saturated concentration of an OOM determines whether it can condense onto particulate matter or not. Due to the Kelvin effect, lower volatility is required for OOMs to condense onto smaller particles. According to the measured OOMs concentration in Beijing, OOMs with $\log_{10}(c^*) \geq 1$ could hardly condense on particles smaller than 25 nm (Fig. S16). Therefore, we define OOMs with $\log_{10}(c^*) \leq 0$ as condensable OOMs, most of which are extremely low-volatility organic compounds (ELVOC, c* in 10^{-8}-10^{-4} $\mu g \cdot m^3$) and low-volatility organic compounds (LVOC, c* in 10^{-4}-10^{-1} $\mu g \cdot m^3$).[44]

2.4 Vapor condensation growth rate simulation

The condensation growth rate (GR), defined as GR = dd_p/dt, represents the change in particle size per unit time. The particle growth rate contributed by OOM condensation for a given diameter was calculated as Eq. 4,[19, 46] and GR for a particle size bin is calculated by averaging the GR of all the particles in this bin.

$$\frac{\mathrm{d}d_p}{\mathrm{d}t} = \left(\frac{d_p + d_i}{d_p}\right)^2 \frac{\bar{c}_{i,p}}{2\rho} \alpha_{i,p} B_{i,p} [C_i^v - a_{i,p} C_i^0] \qquad \text{Eq. (4)}$$

where d_p, d_i are the diameter of the particle and the condensable vapor, respectively; $\bar{c}_{i,p}$is the mean relative thermal velocity between a condensable vapor molecular and a particle; ρ is the density of the particles; $\alpha_{i,p}$ is the accommodation coefficient; $B_{i,p}$ is the Kinetic oriented transition-regime diffusion correction factor. The detailed calculations and assumptions of the above parameters are in SI.

The square bracket term in Eq. 4 represents the driving force of OOM condensation, i.e. the over-saturated concentration of the condensable vapor. C_i^v and C_i^0 are the actual vapor concentration and saturation vapor concentration, respectively. $a_{i,p}$ is the particulate-phase activity, and $a_{i,p} = X_{i,p}\gamma_{i,p}$ $K_{i,p}$, where $\gamma_{i,p}$ is the mass-based activity coefficient in the organic condensed phase, which is assumed to be 1. $K_{i,p}$ is the Kelvin coefficient, which is estimated by $K_{i,p} = 10^{d_{pK}/d_p}$. Assuming a particle surface tension of 0.034 N · m^{-1},[47, 48] and a mean molar weight of 250 g · mol^{-1} at 300 K, the corresponding Kelvin diameter (d_{pK}) is 5 nm. $X_{i,p}$ is the mass fraction of OOM_i at the particle size of d_p. In this study, $X_{i,p}$ changes along with the growth of a new particle, and it was estimated by simulating the cumulative mass of OOM_i in the particulate phase based on the mass flux of OOM_i condensation.

The condensation growth rates contributed by H_2SO_4 and $(H_2SO_4)_n(DMA)_n$ are calculated following the method reported by Stolzenburg et al.,[9] which includes the effect of van der Waals forces in vapour condensation. The details of the calculation are supplemented in the SI.

It should be noted that the theoretical GR in Eq. 4 has a corresponding relationship with particle sizes (d_p) and time (t). For a particle size bin, e.g. 1.5-3 nm, the period used to calculate the

theoretical $GR_{1.5\text{-}3}$ is consistent with that of observed $GR_{1.5\text{-}3}$ with log-normal distribution function method.[49] The time windows used for GR calculations are the exact periods when NPF events occur and develop. The criteria to identified NPF events and the calculation of observed GR is consistent with a previous study.[10]

3 Results and discussion

3.1 OOMs observed in urban Beijing

An overall of ~1100 organic formulas were identified within the m/z range of 200-450 Th for each season. The observed OOMs species in four seasons are generally similar in terms of the total number of identified molecules and the proportion of non-nitrogen OOM molecules (Fig. S1). The mass-defect plot of the averaged OOMs in spring is shown in Fig. 1 as an example.

Several groups of homologues were observed in both non-nitrogen OOMs and nitrogen-containing OOMs. Points lined on the direction of $+CH_2$ are homologues, differed by an integral number of $–CH_2–$ group. The multiple series of homologous oxidation products are likely a result of the co-existed homologues precursors in urban areas, e.g. benzene, toluene, and xylene.[50]

==========

Place Figure 1 Here

==========

Another important feature of OOMs in Beijing is the higher proportion of nitrogen-containing OOMs in comparison to that of forested area (Figs. S2 & S3). In our measurements, ~30% of the identified molecules are non-nitrogen OOMs and ~70% are nitrogen-containing OOMs. Among them, 35-52% of the total concentration of nitrogen-containing OOMs are OOMs with more than one nitrogen atom. The termination of auto-oxidation chain propagation by NO_x results in carbonyl (RO_2+NO reaction) or nitrate functional group (RO_2+NO_x reaction).[14] Multi-generation oxidation of RO_2+NO_x may explain the formation of OOMs with more than one nitrogen atom. Nitrate radical (NO_3) oxidation may also play a role. In addition to the high proportion of nitrogen-

containing OOMs, strong auto-oxidation processes with more than two consecutive oxygen additions are rarely observed; this is consistent with NO_x reactions shortening RO_2 lifetimes in the urban environment.

Although the OOM speciation in each season is quite similar, the total concentration of OOMs in Beijing shows clear seasonal variations while falling within a similar range to concentrations observed elsewhere. As shown in Fig. 2, the seasonal median concentration of total OOMs in Beijing is the highest in summer (4.0×10^8 cm^{-3}), followed by spring (3.3×10^8 cm^{-3}), autumn (1.1×10^8 cm^{-3}), and winter (3.2×10^7 cm^{-3}). Similarly, the concentration of condensable OOMs in urban Beijing, accounting for 17-35% of total OOM concentration, also has the same seasonal variations. The high total OOM concentration in summer is most likely related to the enhanced photochemistry due to stronger solar radiation and higher temperature (Fig. S8). From a global perspective, OOMs measured by nitrate CI-APi-ToF range from 10^7 to 10^9 cm^{-3}. It should be noted that, nitrated phenols can contribute to 14-78% of the total OOM concentration in urban Beijing, which is higher than their contribution of ~16% in those remote forest areas.[51] However, as nitrated phenols are too volatile to have significant contribution to particle growth, they are excluded in the following discussion. The information of identified nitrated phenol peaks is supplemented in the SI.

==========

Place Figure 2 Here

==========

The concentrations of both non-nitrogen OOMs and nitrogen-containing OOMs increase along with solar radiation (UVB) in the morning, which also coincides with particle growth processes. Such patterns are consistent during all four seasons (Fig. S4). The averaged diurnal variations in summer are shown in Fig. 3 as an example. Sulfuric acid starts to rise at around 5 am (local time) and reaches a peak at around 10 am. Both non-nitrogen OOMs and nitrogen-containing OOMs start to rise at 6 am; nitrogen-containing OOMs reach a peak at 11 am and non-nitrate OOMs

reached the peak one hour later. In daytime, OOMs increase along with the increase of solar radiation due to photochemistry, and decrease more slowly than sulfuric acid. This slower decrease of OOMs can be attributed to the continuing formation via ozone oxidation and the lower removal efficiency via condensation onto particles compared to sulfuric acid; it will be discussed in Section 3.2. In addition, the secondary peak of nitrogen-containing OOMs at around 10 pm may be due to the onset of NO_3 chemistry at nighttime.

==========

Place Figure 3 Here

==========

3.2 Particle growth contributed by OOMs condensation

The growth rates of 1.5-25 nm particles driven by condensation of OOMs are approximately 0.25-3.4 $nm \cdot h^{-1}$, and show clear seasonal variations. As shown in Fig. 4, the condensation rates of OOMs, i.e., the sum of non-nitrate and nitrate OOMs, are the highest in summer, ranging from 1.7-3.4 $nm \cdot h^{-1}$, followed by 0.7-2.0 $nm \cdot h^{-1}$ of spring, 0.96-1.48 $nm \cdot h^{-1}$ of autumn, and 0.25-0.3 $nm \cdot h^{-1}$ of winter. For particles in the same size range, the growth rates contributed by OOMs in summer can be 6.5-13 times of those in winter. In addition, the contribution of nitrogen-containing OOMs to particle growth is larger than that of non-nitrate HOMs in all size ranges and all four seasons, with calculated growth rates of 0.2-2.6 $nm \cdot h^{-1}$ and 0.05-0.9 $nm \cdot h^{-1}$, respectively. Moreover, particle growth contributed by sulfuric acid and its clusters, nitrogen-containing OOMs, and non-nitrate OOMs have different size dependencies. With increasing particle diameter, the contribution by OOMs shows a flat or increasing trend, while the contribution by sulfuric acid considerably decreases. Taking summer as an example, from 1.5-3 nm to 15-25 nm, the contribution of sulfuric acid and its clusters decreased from 2.95 to 1.18 $nm \cdot h^{-1}$, nitrogen-containing OOMs increased from 1.03 to 2.76 $nm \cdot h^{-1}$, and non-nitrogen OOMs increased from 0.78 to 1.0 $nm \cdot h^{-1}$.

==========

Place Figure 4 Here

==========

The difference of condensation growth rates during four seasons is primarily due to the strong seasonal variation of the condensable OOM concentration. As shown in Figs. 5a & b, the condensation growth rate contributed by OOMs correlated well (Pearson correlation coefficient of 0.95-0.99 in linear scale) with the condensable OOM concentration for each particle size range (Fig. S10). This is because that the volatility distributions of both non-nitrogen OOMs and nitrogen-containing OOMs are relatively stable in four seasons (Fig. S11). Therefore, for any given particle size, the driving force of particle growth is almost solely determined by the gas-phase concentration of condensable OOMs. As shown in Fig. 6, the concentrations of both non-nitrogen OOMs and nitrogen-containing OOMs vary by almost one order of magnitude, leading to similar extent of variations in particle growth rate.

==========

Place Figure 5 Here

==========

==========

Place Figure 6 Here

==========

In addition to vapor concentration, the effectiveness of vapor condensation also influences the contribution of a certain gaseous species to particle growth. Here, we use the term "growth promotion efficiency (GPE)", defined as the resulted growth rate per unit concentration (e.g., $nm \cdot h^{-1}/cm^{-3}$). From this perspective, sulfuric acid and its clusters are the most efficient condensable vapors, followed by non-nitrate OOMs and nitrogen-containing OOMs (Fig. 5c). The GPE is

essentially determined by the bulk volatility and the averaged molar mass of different species.[52] Sulfuric acid, although with a small molar mass, can hardly evaporate, so that it has the highest efficiency. For the case of OOMs, non-nitrogen OOMs and nitrogen-containing OOMs have similar molar mass, but the bulk volatility of non-nitrate OOMs is lower than that of nitrogen-containing OOMs (Figs. S12-13). Therefore, the GPE of non-nitrate OOMs is higher than that of nitrogen-containing OOMs, and with the same vapor concentration, non-nitrate OOMs lead to larger growth rates than nitrogen-containing OOMs do.

Taking both the vapor concentration and GPE into consideration, we could explain the difference of condensation growth rate between non-nitrogen OOMs and nitrogen-containing OOMs. The total concentrations of condensable nitrogen-containing OOMs are 2.67-3.37 times of non-nitrogen OOMs (Fig. 6), but the lower GPE of nitrogen-containing OOMs (Fig. 5c) partially offsets the higher concentration. As a whole, the growth rates contributed by nitrogen-containing OOMs are 1-2.33 times of that by non-nitrogen OOMs.

As also shown in Fig.5c, the GPE of different species varies differently across particle sizes. For sulfuric acid and its clusters, their GPE decrease with increased particle sizes. This is because condensation of same amount of sulfuric acid causes smaller increases in diameters for large particles than for small particles. Similar effect is expected for OOMs, however, OOM condensation is also strongly influenced by the Kelvin effect. More OOMs can condense as particles grow larger and the Kelvin effect diminishes, which compensates the size effect and leads to an overall weak size dependence.

4 Atmospheric implications

This study reports the seasonal characteristics of OOMs in an urban environment and supplements for the global scheme[14], which helps to better understand OOMs formation in different environments. We found an atmospheric relevance between solar radiation and OOMs concentration in a seasonal scale: with the increase of solar radiation intensity (from winter to summer), the concentration of day-time OOMs rises rapidly first and then increases slowly (Fig. S8a). The strength of solar radiation is correlated with OH radical concentration and atmospheric temperature.[53, 54] Since the concentration of precursors in winter is not significantly lower than other seasons (Fig. S9a) and its loss through condensation sink is not higher than other seasons

(Fig. S9c), the lower oxidant concentrations (e.g. OH radical) and lower temperature may substantially limit the formation of OOMs in wintertime. Compared with the seasonal variations of VOC precursors and condensation sink, photochemical strength seems to play a more important role in the seasonal variation of OOM concentrations based on its better consistency (Fig. S9). This correlation may also exist in other mid-latitude urban and forested environments that with distinct seasonal changes.

In urban Beijing, sulfuric acid and its clusters can explain a significant fraction of the observed growth of 1.5-3 nm particles[10], and OOMs have a significant contribution to the growth of 3-25 nm particles (Fig. 7). The higher contribution of sulfuric acid and its clusters in 1.5-3 nm particles can be explained by its high GPE at this size range (Fig. 5c). In addition, the concentration of sulfuric acid rises early and steeply during the time window when the initial growth of new particles occurs (Fig. 3). For larger (3-25 nm) particles, despite the lower GPE of OOMs than sulfuric acid, OOMs start to dominate particle growth, due to the much higher vapor concentration and the increasingly weaker Kelvin effect. Overall, the contributions by sulfuric acid and OOMs can explain a major fraction of the observed growth rate in all size ranges of 1.5-25 nm.

It was reported that NPF events in Beijing can contribute to the surface area concentration and mass concentration of atmospheric aerosols (mainly governed by particles larger than 100 nm), especially under conditions with a fast growth of newly formed particles.[5, 55] Although this study focused on the growth of nanoparticles, the condensation of OOMs is expected to contribute significantly to the growth of large particles as well.

However, winter is an exception. A clear discrepancy remains between simulated and observed growth rate in 3-25 nm particles, which may be an indication of some missing contributors. One plausible cause is the underestimation of condensable OOM concentration at low temperatures. Nitrate CI-APi-ToF is less sensitive to moderately oxidized molecules,[56] while with the decrease of temperature, some moderately oxidized organics may become condensable and contribute to particle growth.[57] Meanwhile, particle-phase processes could promote particle growth through lowering the volatility of particles-phase organics,[58] including condensed phase reactions and oligomerization.[59] Another possible reasons is the missing contribution by HNO_3 and NH_3 at low temperatures, as suggested by a recent chamber study.[60]

==========

Place Figure 7 Here

==========

In some cases, the simulated particle growth rates are higher than observed values (Fig. 7). This may arise from two sources of uncertainties. One is the uncertainty in growth rate simulation, which mainly comes from the estimation of OOMs volatility (Fig. S5). The other is from the calculation of observed growth rate. As illustrated by Deng et al.,[10] growth rates calculated using the appearance time method and the log-normal distribution method can sometimes differ by a factor of 2. We investigated the results of appearance time growth rate and corrected the influence by particle coagulation[61] (Figs. S14-15). The ratios of simulated growth rate over observed growth rate are lower when particle growth rates are calculated with the appearance time method. However, our findings on the important role of OOMs in explaining the growth rate of 3-25 nm particles remain valid. In addition, the sum of OOMs, sulfuric acid and its clusters is still far from explaining the observed growth rate (appearance time method) in winter.

Supporting Information

It includes the detailed information on the calculation method of simulated growth rate; comparison of observed oxygenated organic molecules in all of the four seasons using Venn plot (Figure S1); the proportion of carbon-resolved non-nitrogen OOMs and nitrogen-containing OOMs in Beijing and other atmospheric environment (Figures S2 & S3); the diurnal variation of sulfuric acid, non-nitrogen OOMs and nitrogen-containing OOMs in all of the four seasons (Figure S4); the comparison of two volatility parameterization methods (Figure S5); the volatility distribution of observed oxygenated organic molecules (OOMs) in Beijing for four seasons (Figure S6); the relations between H to C ratio and O to C ratio of known OOMs peaklists from laboratory

studies (Figure S7); the relations of condensable oxygenated organic molecules with temperature and solar radiation (Figure S8); seasonal variations of volatile organic compounds, temperature and solar radiation, and condensation sink (CS) in Beijing (Figure S9); relations of size-resolved simulated growth rate and condensing vapor concentration (Figure S10); the relations of driving force and OOMs concentration (Figure S11); the growth efficiency of different kinds of condensing vapors (Figure S12); the volatility distribution of non-nitrogen OOMs and nitrogen-containing OOMs (Figure S13); the relations of simulated GR and observed GR (appearance time method) for different particle size bins (Figures S14 & S15); the condensation growth rate contributed by OOMs with different volatilities for 1.5-25 nm particles (Figure S16); six examples for peak identification in tofTool (Figure S17); concentration of total OOMs in new particle formation (NPF) days and non-NPF days. (Figure S18); and the identified nitrated phenol peaks during the measurement (Table S1).

AUTHOR INFORMATION

Corresponding Author

* **Jingkun Jiang** − State Key Joint Laboratory of Environment Simulation and Pollution Control, School of Environment, Tsinghua University, 100084 Beijing, China; Email: jiangjk@tsinghua.edu.cn

* **Chao Yan** − Institute for Atmospheric and Earth System Research Physics, Faculty of Science, University of Helsinki, 00014 Helsinki, Finland; Aerosol and Haze Laboratory, Beijing Advanced Innovation Center for Soft Matter Science and Engineering, Beijing University of Chemical Technology, 100029 Beijing, China; Email: chao.yan@helsinki.fi

Notes

The authors declare no competing financial interest.

Acknowledgement

Financial support from the National Science Foundation of China (92044301, 21876094, and 41730106) and Samsung $PM_{2.5}$ SRP are acknowledged.

Reference

1. Kulmala, M.; Vehkamäki, H.; Petäjä, T.; Dal Maso, M.; Lauri, A.; Kerminen, V. M.; Birmili, W.; McMurry, P. H., Formation and growth rates of ultrafine atmospheric particles: A review of observations. *Journal of Aerosol Science* **2004,** *35*, 143-176.

2. Kerminen, V. M.; Lihavainen, H.; Komppula, M.; Viisanen, Y.; Kulmala, M., Direct observational evidence linking atmospheric aerosol formation and cloud droplet activation. *Geophysical Research Letters* **2005,** *32*, 1-4.

3. Merikanto, J.; Spracklen, D. V.; Mann, G. W.; Pickering, S. J.; Carslaw, K. S., Impact of nucleation on global CCN. *Atmospheric Chemistry and Physics* **2009,** *9*, 8601-8616.

4. McMurry, P. H.; Friedlander, S. K., New particle formation in the presence of an aerosol. *Atmospheric Environment* **1979,** *13*, (12), 1635-1651.

5. Guo, S.; Hu, M.; Zamora, M. L.; Peng, J.; Shang, D.; Zheng, J.; Du, Z.; Wu, Z.; Shao, M.; Zeng, L.; Molina, M. J.; Zhang, R., Elucidating severe urban haze formation in China. *Proceedings of the National Academy of Sciences of the United States of America* **2014,** *111*, 17373-17378.

6. Cai, R. L.; Yang, D. S.; Fu, Y. Y.; Wang, X.; Li, X. X.; Ma, Y.; Hao, J. M.; Zheng, J.; Jiang, J. K., Aerosol surface area concentration: a governing factor in new particle formation in Beijing. *Atmospheric Chemistry and Physics* **2017,** *17*, (20), 12327-12340.

7. Kulmala, M.; Kerminen, V. M.; Petäjä, T.; Ding, A. J.; Wang, L., Atmospheric gas-to-particle conversion: Why NPF events are observed in megacities? *Faraday Discussions* **2017,** *200*, 271-288.

8. McMurry, P. H.; Fink, M.; Sakurai, H.; Stolzenburg, M. R.; Mauldin, I. L.; Smith, J.; Eisele, F.; Moore, K.; Sjostedt, S.; Tanner, D.; Huey, L. G.; Nowak, J. B.; Edgerton, E.; Voisin, D., A criterion for new particle formation in the sulfur-rich Atlanta atmosphere. *Journal of Geophysical Research Atmospheres* **2005,** *110*, 1-10.

9. Stolzenburg, D.; Simon, M.; Ranjithkumar, A.; Kürten, A.; Lehtipalo, K.; Gordon, H.; Ehrhart, S.; Finkenzeller, H.; Pichelstorfer, L.; Nieminen, T.; He, X.-C.; Brilke, S.; Xiao, M.; Amorim, A.; Baalbaki, R.; Baccarini, A.; Beck, L.; Bräkling, S.; Caudillo Murillo, L.; Chen, D.; Chu, B.; Dada, L.; Dias, A.; Dommen, J.; Duplissy, J.; El Haddad, I.; Fischer, L.; Gonzalez Carracedo, L.; Heinritzi, M.; Kim, C.; Koenig, T. K.; Kong, W.; Lamkaddam, H.; Lee, C. P.; Leiminger, M.; Li, Z.; Makhmutov, V.; Manninen, H. E.; Marie, G.; Marten, R.; Müller, T.; Nie, W.; Partoll, E.; Petäjä, T.; Pfeifer, J.; Philippov, M.; Rissanen, M. P.; Rörup, B.; Schobesberger, S.; Schuchmann, S.; Shen, J.; Sipilä, M.; Steiner, G.; Stozhkov, Y.; Tauber, C.; Tham, Y. J.; Tomé, A.; Vazquez-Pufleau, M.; Wagner, A. C.; Wang, M.; Wang, Y.; Weber, S. K.; Wimmer, D.; Wlasits, P. J.; Wu, Y.; Ye, Q.; Zauner-Wieczorek, M.; Baltensperger, U.; Carslaw, K. S.; Curtius, J.; Donahue, N. M.; Flagan, R. C.; Hansel, A.; Kulmala, M.; Lelieveld, J.; Volkamer, R.; Kirkby, J.; Winkler, P. M., Enhanced growth rate of atmospheric particles from sulfuric acid. *Atmospheric Chemistry and Physics* **2020,** *20*, (12), 7359-7372.

10. Deng, C.; Fu, Y.; Dada, L.; Yan, C.; Cai, R.; Yang, D.; Zhou, Y.; Yin, R.; Lu, Y.; Li, X.; Qiao, X.; Fan, X.; Nie, W.; Kontkanen, J.; Kangasluoma, J.; Chu, B.; Ding, A.; Kerminen, V. M.; Paasonen, P.; Worsnop, D. R.; Bianchi, F.; Liu, Y.; Zheng, J.; Wang, L.; Kulmala, M.; Jiang, J., Seasonal Characteristics of New Particle Formation and Growth in Urban Beijing. *Environmental Science & Technology* **2020,** *54*, (14), 8547-8557.

11. Stolzenburg, M. R.; McMurry, P. H.; Sakurai, H.; Smith, J. N.; Mauldin, R. L.; Eisele, F. L.; Clement, C. F., Growth rates of freshly nucleated atmospheric particles in Atlanta. *Journal of Geophysical Research Atmospheres* **2005,** *110*, 1-10.

12. Riipinen, I.; Yli-Juuti, T.; Pierce, J. R.; Petäjä, T.; Worsnop, D. R.; Kulmala, M.; Donahue, N. M., The contribution of organics to atmospheric nanoparticle growth. *Nature Geoscience* **2012,** *5*, 453-458.

13. Mohr, C.; Thornton, J. A.; Heitto, A.; Lopez-Hilfiker, F. D.; Lutz, A.; Riipinen, I.; Hong, J.; Donahue, N. M.; Hallquist, M.; Petäjä, T.; Kulmala, M.; Yli-Juuti, T., Molecular identification of organic vapors driving atmospheric nanoparticle growth. *Nature Communications* **2019,** *10*, 1-7.

14. Bianchi, F.; Kurten, T.; Riva, M.; Mohr, C.; Rissanen, M. P.; Roldin, P.; Berndt, T.; Crounse, J. D.; Wennberg, P. O.; Mentel, T. F.; Wildt, J.; Junninen, H.; Jokinen, T.; Kulmala, M.; Worsnop, D. R.; Thornton, J. A.; Donahue, N.; Kjaergaard, H. G.; Ehn, M., Highly Oxygenated Organic Molecules (HOM) from Gas-Phase Autoxidation Involving Peroxy Radicals: A Key Contributor to Atmospheric Aerosol. *Chemical Reviews* **2019,** *119*, (6), 3472-3509.

15. Molteni, U.; Bianchi, F.; Klein, F.; El Haddad, I.; Frege, C.; Rossi, M. J.; Dommen, J.; Baltensperger, U., Formation of highly oxygenated organic molecules from aromatic compounds. *Atmospheric Chemistry and Physics* **2018,** *18*, 1909-1921.

16. Jokinen, T.; Kausiala, O.; Garmash, O.; Peräkylä, O.; Junninen, H.; Schobesberger, S.; Yan, C.; Sipilä, M.; Rissanen, M. P., Production of highly oxidized organic compounds from ozonolysis of β-caryophyllene: Laboratory and field measurements. *Boreal Environment Research* **2016,** *21*, 262-273.

17. Lee, A.; Goldstein, A. H.; Kroll, J. H.; Ng, N. L.; Varutbangkul, V.; Flagan, R. C.; Seinfeld, J. H., Gas-phase products and secondary aerosol yields from the photooxidation of 16 different terpenes. *Journal of Geophysical Research Atmospheres* **2006,** *111*, 1-25.

18. Ehn, M.; Thornton, J. A.; Kleist, E.; Sipila, M.; Junninen, H.; Pullinen, I.; Springer, M.; Rubach, F.; Tillmann, R.; Lee, B.; Lopez-Hilfiker, F.; Andres, S.; Acir, I. H.; Rissanen, M.; Jokinen, T.; Schobesberger, S.; Kangasluoma, J.; Kontkanen, J.; Nieminen, T.; Kurten, T.; Nielsen, L. B.; Jorgensen, S.; Kjaergaard, H. G.; Canagaratna, M.; Maso, M. D.; Berndt, T.; Petaja, T.; Wahner, A.; Kerminen, V. M.; Kulmala, M.; Worsnop, D. R.; Wildt, J.; Mentel, T. F., A large source of low-volatility secondary organic aerosol. *Nature* **2014,** *506*, 476-479.

19. Tröstl, J.; Chuang, W. K.; Gordon, H.; Heinritzi, M.; Yan, C.; Molteni, U.; Ahlm, L.; Frege, C.; Bianchi, F.; Wagner, R.; Simon, M.; Lehtipalo, K.; Williamson, C.; Craven, J. S.; Duplissy, J.; Adamov, A.; Almeida, J.; Bernhammer, A. K.; Breitenlechner, M.; Brilke, S.; Dias, A.; Ehrhart, S.; Flagan, R. C.; Franchin, A.; Fuchs, C.; Guida, R.; Gysel, M.; Hansel, A.; Hoyle, C. R.; Jokinen, T.; Junninen, H.; Kangasluoma, J.; Keskinen, H.; Kim, J.; Krapf, M.; Kurten, A.; Laaksonen, A.; Lawler, M.; Leiminger, M.; Mathot, S.; Mohler, O.; Nieminen, T.; Onnela, A.; Petaja, T.; Piel, F. M.; Miettinen, P.; Rissanen, M. P.; Rondo, L.; Sarnela, N.; Schobesberger, S.; Sengupta, K.; Sipila, M.; Smith, J. N.; Steiner, G.; Tome, A.; Virtanen, A.; Wagner, A. C.; Weingartner, E.; Wimmer, D.; Winkler, P. M.; Ye, P.; Carslaw, K. S.; Curtius, J.; Dommen, J.; Kirkby, J.; Kulmala, M.; Riipinen, I.; Worsnop, D. R.; Donahue, N. M.; Baltensperger, U., The

485 role of low-volatility organic compounds in initial particle growth in the atmosphere. *Nature*
486 **2016,** *533*, (7604), 527-31.
487 20. Kirkby, J.; Duplissy, J.; Sengupta, K.; Frege, C.; Gordon, H.; Williamson, C.; Heinritzi,
488 M.; Simon, M.; Yan, C.; Almeida, J.; Trostl, J.; Nieminen, T.; Ortega, I. K.; Wagner, R.;
489 Adamov, A.; Amorim, A.; Bernhammer, A. K.; Bianchi, F.; Breitenlechner, M.; Brilke, S.; Chen,
490 X.; Craven, J.; Dias, A.; Ehrhart, S.; Flagan, R. C.; Franchin, A.; Fuchs, C.; Guida, R.; Hakala,
491 J.; Hoyle, C. R.; Jokinen, T.; Junninen, H.; Kangasluoma, J.; Kim, J.; Krapf, M.; Kurten, A.;
492 Laaksonen, A.; Lehtipalo, K.; Makhmutov, V.; Mathot, S.; Molteni, U.; Onnela, A.; Perakyla,
493 O.; Piel, F.; Petaja, T.; Praplan, A. P.; Pringle, K.; Rap, A.; Richards, N. A.; Riipinen, I.;
494 Rissanen, M. P.; Rondo, L.; Sarnela, N.; Schobesberger, S.; Scott, C. E.; Seinfeld, J. H.; Sipila,
495 M.; Steiner, G.; Stozhkov, Y.; Stratmann, F.; Tome, A.; Virtanen, A.; Vogel, A. L.; Wagner, A.
496 C.; Wagner, P. E.; Weingartner, E.; Wimmer, D.; Winkler, P. M.; Ye, P.; Zhang, X.; Hansel, A.;
497 Dommen, J.; Donahue, N. M.; Worsnop, D. R.; Baltensperger, U.; Kulmala, M.; Carslaw, K. S.;
498 Curtius, J., Ion-induced nucleation of pure biogenic particles. *Nature* **2016,** *533*, 521-526.
499 21. Schobesberger, S.; Junninen, H.; Bianchi, F.; Lonn, G.; Ehn, M.; Lehtipalo, K.; Dommen,
500 J.; Ehrhart, S.; Ortega, I. K.; Franchin, A.; Nieminen, T.; Riccobono, F.; Hutterli, M.; Duplissy,
501 J.; Almeida, J.; Amorim, A.; Breitenlechner, M.; Downard, A. J.; Dunne, E. M.; Flagan, R. C.;
502 Kajos, M.; Keskinen, H.; Kirkby, J.; Kupc, A.; Kurten, A.; Kurten, T.; Laaksonen, A.; Mathot,
503 S.; Onnela, A.; Praplan, A. P.; Rondo, L.; Santos, F. D.; Schallhart, S.; Schnitzhofer, R.; Sipila,
504 M.; Tome, A.; Tsagkogeorgas, G.; Vehkamaki, H.; Wimmer, D.; Baltensperger, U.; Carslaw, K.
505 S.; Curtius, J.; Hansel, A.; Petaja, T.; Kulmala, M.; Donahue, N. M.; Worsnop, D. R., Molecular
506 understanding of atmospheric particle formation from sulfuric acid and large oxidized organic
507 molecules. *Proceedings of the National Academy of Sciences of the United States of America*
508 **2013,** *110*, (43), 17223-8.
509 22. Zhao, J.; Ortega, J.; Chen, M.; McMurry, P. H.; Smith, J. N., Dependence of particle
510 nucleation and growth on high molecular weight gas phase products during ozonolysis of α-
511 pinene. *Atmospheric Chemistry and Physics* **2013,** *13*, 7631-7644.
512 23. Crounse, J. D.; Nielsen, L. B.; Jørgensen, S.; Kjaergaard, H. G.; Wennberg, P. O.,
513 Autoxidation of organic compounds in the atmosphere. *Journal of Physical Chemistry Letters*
514 **2013,** *4*, 3513-3520.

515 24. Wang, S.; Riva, M.; Yan, C.; Ehn, M.; Wang, L., Primary Formation of Highly Oxidized
516 Multifunctional Products in the OH-Initiated Oxidation of Isoprene: A Combined Theoretical
517 and Experimental Study. *Environmental Science and Technology* **2018,** *52*, 12255-12264.
518 25. Krechmer, J. E.; Coggon, M. M.; Massoli, P.; Nguyen, T. B.; Crounse, J. D.; Hu, W.;
519 Day, D. A.; Tyndall, G. S.; Henze, D. K.; Rivera-Rios, J. C.; Nowak, J. B.; Kimmel, J. R.;
520 Mauldin, R. L., 3rd; Stark, H.; Jayne, J. T.; Sipila, M.; Junninen, H.; Clair, J. M.; Zhang, X.;
521 Feiner, P. A.; Zhang, L.; Miller, D. O.; Brune, W. H.; Keutsch, F. N.; Wennberg, P. O.; Seinfeld,
522 J. H.; Worsnop, D. R.; Jimenez, J. L.; Canagaratna, M. R., Formation of Low Volatility Organic
523 Compounds and Secondary Organic Aerosol from Isoprene Hydroxyhydroperoxide Low-NO
524 Oxidation. *Environmental Science & Technology* **2015,** *49*, (17), 10330-9.
525 26. Garmash, O.; Rissanen, M. P.; Pullinen, I.; Schmitt, S.; Kausiala, O.; Tillmann, R.; Zhao,
526 D.; Percival, C.; Bannan, T. J.; Priestley, M.; Hallquist, A. M.; Kleist, E.; Kiendler-Scharr, A.;
527 Hallquist, M.; Berndt, T.; McFiggans, G.; Wildt, J.; Mentel, T. F.; Ehn, M., Multi-generation OH
528 oxidation as a source for highly oxygenated organic molecules from aromatics. *Atmospheric*
529 *Chemistry and Physics* **2020,** *20*, 515-537.
530 27. Rissanen, M. P., NO2 Suppression of Autoxidation-Inhibition of Gas-Phase Highly
531 Oxidized Dimer Product Formation. *ACS Earth and Space Chemistry* **2018,** *2*, 1211-1219.
532 28. Xiao, M.; Hoyle, C.; Dada, L.; Stolzenburg, D.; Kürten, A.; Wang, M.; Lamkaddam, H.;
533 Garmash, O.; Mentler, B.; Molteni, U.; Baccarini, A.; Simon, M.; He, X.-C.; Lehtipalo, K.;
534 Ahonen, L.; Baalbaki, R.; Bauer, P.; Beck, L.; Bell, D.; Bianchi, F.; Brilke, S.; Chen, D.; Chiu,
535 R.; Dias, A.; Duplissy, J.; Finkenzeller, H.; Gordon, H.; Hofbauer, V.; Kim, C.; Koenig, T.;
536 Lampilahti, J.; Lee, C. P.; Li, Z.; Mai, H.; Makhmutov, V.; Manninen, H.; Marten, R.; Mathot,
537 S.; Mauldin, R.; Nie, W.; Onnela, A.; Partoll, E.; Petäjä, T.; Pfeifer, J.; Pospisilova, V.;
538 Quéléver, L.; Rissanen, M.; Schobesberger, S.; Schuchmann, S.; Stozhkov, Y.; Tauber, C.;
539 Tham, Y. J.; Tomé, A.; Vazquez-Pufleau, M.; Wagner, A.; Wanger, R.; Wang, Y.; Weitz, L.;
540 Wimmer, D.; Wu, Y.; Yan, C.; Ye, P.; Ye, Q.; Zha, Q.; Zhou, X.; Amorim, A.; Carslaw, K.;
541 Curtius, J.; Hansel, A.; Volkamer, R.; Winkler, P.; Flagan, R.; Kulmala, M.; Worsnop, D.;
542 Kirkby, J.; Donahue, N.; Baltensperger, U.; El Haddad, I.; Dommen, J., The driving factors of
543 new particle formation and growth in the polluted boundary layer. *Atmospheric Chemistry and*
544 *Physics Discussions* **2021**, https://doi.org/10.5194/acp-2020-1323.
545 29. Yan, C.; Nie, W.; Vogel, A. L.; Dada, L.; Lehtipalo, K.; Stolzenburg, D.; Wagner, R.;
546 Rissanen, M. P.; Xiao, M.; Ahonen, L.; Fischer, L.; Rose, C.; Bianchi, F.; Gordon, H.; Simon,

547 M.; Heinritzi, M.; Garmash, O.; Roldin, P.; Dias, A.; Ye, P.; Hofbauer, V.; Amorim, A.; Bauer,
548 P. S.; Bergen, A.; Bernhammer, A. K.; Breitenlechner, M.; Brilke, S.; Buchholz, A.; Mazon, S.
549 B.; Canagaratna, M. R.; Chen, X.; Ding, A.; Dommen, J.; Draper, D. C.; Duplissy, J.; Frege, C.;
550 Heyn, C.; Guida, R.; Hakala, J.; Heikkinen, L.; Hoyle, C. R.; Jokinen, T.; Kangasluoma, J.;
551 Kirkby, J.; Kontkanen, J.; Kurten, A.; Lawler, M. J.; Mai, H.; Mathot, S.; Mauldin, R. L., 3rd;
552 Molteni, U.; Nichman, L.; Nieminen, T.; Nowak, J.; Ojdanic, A.; Onnela, A.; Pajunoja, A.;
553 Petaja, T.; Piel, F.; Quelever, L. L. J.; Sarnela, N.; Schallhart, S.; Sengupta, K.; Sipila, M.; Tome,
554 A.; Trostl, J.; Vaisanen, O.; Wagner, A. C.; Ylisirnio, A.; Zha, Q.; Baltensperger, U.; Carslaw,
555 K. S.; Curtius, J.; Flagan, R. C.; Hansel, A.; Riipinen, I.; Smith, J. N.; Virtanen, A.; Winkler, P.
556 M.; Donahue, N. M.; Kerminen, V. M.; Kulmala, M.; Ehn, M.; Worsnop, D. R., Size-dependent
557 influence of NOx on the growth rates of organic aerosol particles. *Science Advances* 2020, *6*,
558 (22), 4945.
559 30. Yan, C.; Yin, R. J.; Lu, Y. Q.; Dada, L. N.; Yang, D. S.; Fu, Y. Y.; Kontkanen, J.; Deng,
560 C. J.; Garmash, O.; Ruan, J. X.; Baalbaki, R.; Schervish, M.; Cai, R. L.; Bloss, M.; Chan, T.;
561 Chen, T. Z.; Chen, Q.; Chen, X. M.; Chen, Y.; Chu, B. W.; Dallenbach, K.; Foreback, B.; He, X.
562 C.; Heikkinen, L.; Jokinen, T.; Junninen, H.; Kangasluoma, J.; Kokkonen, T.; Kurppa, M.;
563 Lehtipalo, K.; Li, H. Y.; Li, H.; Li, X. X.; Liu, Y. L.; Ma, Q. X.; Paasonen, P.; Rantala, P.;
564 Pileci, R. E.; Rusanen, A.; Sarnela, N.; Simonen, P.; Wang, S. X.; Wang, W. G.; Wang, Y. H.;
565 Xue, M.; Yang, G.; Yao, L.; Zhou, Y.; Kujansuu, J.; Petaja, T.; Nie, W.; Ma, Y.; Ge, M. F.; He,
566 H.; Donahue, N. M.; Worsnop, D. R.; Kerminen, V. M.; Wang, L.; Liu, Y. C.; Zheng, J.; Kulma,
567 M.; Jiang, J. K.; Bianchi, F., The Synergistic Role of Sulfuric Acid, Bases, and Oxidized
568 Organics Governing New-Particle Formation in Beijing. *Geophysical Research Letters* 2021, *48*,
569 (7), 91944.
570 31. Brean, J.; Harrison, R. M.; Shi, Z. B.; Beddows, D. C. S.; Acton, W. J. F.; Hewitt, C. N.;
571 Squires, F. A.; Lee, J., Observations of highly oxidized molecules and particle nucleation in the
572 atmosphere of Beijing. *Atmospheric Chemistry and Physics* 2019, *19*, (23), 14933-14947.
573 32. Liu, Y.; Yan, C.; Feng, Z.; Zheng, F.; Fan, X.; Zhang, Y.; Li, C.; Zhou, Y.; Lin, Z.; Guo,
574 Y.; Zhang, Y.; Ma, L.; Zhou, W.; Liu, Z.; Dada, L.; Daellenbach, K.; Kontkanen, J.; Cai, R.;
575 Chan, T.; Kulmala, M., Continuous and comprehensive atmospheric observations in Beijing: a
576 station to understand the complex urban atmospheric environment. *Big Earth Data* 2020, *4*, 295-
577 321.

578 33. Jokinen, T.; Sipilä, M.; Junninen, H.; Ehn, M.; Lönn, G.; Hakala, J.; Petäjä, T.; Mauldin,
579 R. L.; Kulmala, M.; Worsnop, D. R., Atmospheric sulphuric acid and neutral cluster
580 measurements using CI-APi-TOF. *Atmospheric Chemistry and Physics* **2012,** *12*, 4117-4125.
581 34. Bertram, T. H.; Kimmel, J. R.; Crisp, T. A.; Ryder, O. S.; Yatavelli, R. L. N.; Thornton,
582 J. A.; Cubison, M. J.; Gonin, M.; Worsnop, D. R., A field-deployable, chemical ionization time-
583 of-flight mass spectrometer. *Atmospheric Measurement Techniques* **2011,** *4*, 1471-1479.
584 35. Heinritzi, M.; Simon, M.; Steiner, G.; Wagner, A. C.; Kürten, A.; Hansel, A.; Curtius, J.,
585 Characterization of the mass-dependent transmission efficiency of a CIMS. *Atmospheric*
586 *Measurement Techniques* **2016,** *9*, 1449-1460.
587 36. Cai, R.; Yan, C.; Yang, D.; Yin, R.; Lu, Y.; Deng, C.; Fu, Y.; Ruan, J.; Li, X.;
588 Kontkanen, J.; Zhang, Q.; Kangasluoma, J.; Ma, Y.; Hao, J.; Worsnop, D. R.; Bianchi, F.;
589 Paasonen, P.; Kerminen, V.-M.; Liu, Y.; Wang, L.; Zheng, J.; Kulmala, M.; Jiang, J., Sulfuric
590 acid–amine nucleation in urban Beijing. *Atmospheric Chemistry and Physics* **2021,** *21*, (4),
591 2457-2468.
592 37. Jiang, J.; Chen, M.; Kuang, C.; Attoui, M.; McMurry, P. H., Electrical Mobility
593 Spectrometer Using a Diethylene Glycol Condensation Particle Counter for Measurement of
594 Aerosol Size Distributions Down to 1 nm. *Aerosol Science and Technology* **2011,** *45*, (4), 510-
595 521.
596 38. Cai, R.; Chen, D.-R.; Hao, J.; Jiang, J., A miniature cylindrical differential mobility
597 analyzer for sub-3 nm particle sizing. *Journal of Aerosol Science* **2017,** *106*, 111-119.
598 39. Liu, J.; Jiang, J.; Zhang, Q.; Deng, J.; Hao, J., A spectrometer for measuring particle size
599 distributions in the range of 3 nm to 10 μm. *Frontiers of Environmental Science & Engineering*
600 **2016,** *10*, (1), 63-72.
601 40. Fu, Y.; Xue, M.; Cai, R.; Kangasluoma, J.; Jiang, J., Theoretical and experimental
602 analysis of the core sampling method: Reducing diffusional losses in aerosol sampling line.
603 *Aerosol Science and Technology* **2019,** *53*, 793-801.
604 41. Cai, R.; Chen, D. R.; Hao, J.; Jiang, J., A miniature cylindrical differential mobility
605 analyzer for sub-3 nm particle sizing. *Journal of Aerosol Science* **2017,** *106*, 111-119.
606 42. Junninen, H.; Ehn, M.; Petäjä; Luosujärvi, L.; Kotiaho, T.; Kostiainen, R.; Rohner, U.;
607 Gonin, M.; Fuhrer, K.; Kulmala, M.; Worsnop, D. R., A high-resolution mass spectrometer to
608 measure atmospheric ion composition. *Atmospheric Measurement Techniques* **2010,** *3*, 1039-
609 1053.

610 43. Kurten, A.; Rondo, L.; Ehrhart, S.; Curtius, J., Calibration of a chemical ionization mass
611 spectrometer for the measurement of gaseous sulfuric acid. *Journal of Physical Chemistry A*
612 **2012,** *116*, 6375-6386.
613 44. Donahue, N. M.; Kroll, J. H.; Pandis, S. N.; Robinson, A. L., A two-dimensional
614 volatility basis set-Part 2: Diagnostics of organic-aerosol evolution. *Atmospheric Chemistry and*
615 *Physics* **2012,** *12*, 615-634.
616 45. Wang, M.; Chen, D.; Xiao, M.; Ye, Q.; Stolzenburg, D.; Hofbauer, V.; Ye, P.; Vogel, A.
617 L.; Mauldin, R. L., 3rd; Amorim, A.; Baccarini, A.; Baumgartner, B.; Brilke, S.; Dada, L.; Dias,
618 A.; Duplissy, J.; Finkenzeller, H.; Garmash, O.; He, X. C.; Hoyle, C. R.; Kim, C.; Kvashnin, A.;
619 Lehtipalo, K.; Fischer, L.; Molteni, U.; Petaja, T.; Pospisilova, V.; Quelever, L. L. J.; Rissanen,
620 M.; Simon, M.; Tauber, C.; Tome, A.; Wagner, A. C.; Weitz, L.; Volkamer, R.; Winkler, P. M.;
621 Kirkby, J.; Worsnop, D. R.; Kulmala, M.; Baltensperger, U.; Dommen, J.; El-Haddad, I.;
622 Donahue, N. M., Photo-oxidation of Aromatic Hydrocarbons Produces Low-Volatility Organic
623 Compounds. *Environmental Science & Technology* **2020,** *54*, (13), 7911-7921.
624 46. Seinfeld, J. H.; Pandis, S. N., *Atmospheric chemistry and physics: from air pollution to*
625 *cliamte change*. 3rd ed.; John Wiley & Sons, Inc.: Hoboken, New Jersey, 2016.
626 47. Fenelonov, V. B.; Kodenyov, G. G.; Kostrovsky, V. G., On the dependence of surface
627 tension of liquids on the curvature of the liquid-vapor interface. *Journal of Physical Chemistry B*
628 **2001,** *105*, 1050-1055.
629 48. Yli-Juuti, T.; Barsanti, K.; Hildebrandt Ruiz, L.; Kieloaho, A. J.; Makkonen, U.; Petäjä,
630 T.; Ruuskanen, T.; Kulmala, M.; Riipinen, I., Model for acid-base chemistry in nanoparticle
631 growth (MABNAG). *Atmospheric Chemistry and Physics* **2013,** *13*, 12507-12524.
632 49. Kulmala, M.; Petäjä, T.; Nieminen, T.; Sipilä, M.; Manninen, H. E.; Lehtipalo, K.; Dal
633 Maso, M.; Aalto, P. P.; Junninen, H.; Paasonen, P.; Riipinen, I.; Lehtinen, K. E. J.; Laaksonen,
634 A.; Kerminen, V. M., Measurement of the nucleation of atmospheric aerosol particles. *Nature*
635 *Protocols* **2012,** *7*, 1651-1667.
636 50. Sheng, J.; Zhao, D.; Ding, D.; Li, X.; Huang, M.; Gao, Y.; Quan, J.; Zhang, Q.,
637 Characterizing the level, photochemical reactivity, emission, and source contribution of the
638 volatile organic compounds based on PTR-TOF-MS during winter haze period in Beijing, China.
639 *Atmospheric Research* **2018,** *212*, 54-63.
640 51. Yan, C.; Nie, W.; Äijälä, M.; Rissanen, M. P.; Canagaratna, M. R.; Massoli, P.; Junninen,
641 H.; Jokinen, T.; Sarnela, N.; Häme, S. A. K.; Schobesberger, S.; Canonaco, F.; Yao, L.; Prévôt,

642 A. S. H.; Petäjä, T.; Kulmala, M.; Sipilä, M.; Worsnop, D. R.; Ehn, M., Source characterization
643 of highly oxidized multifunctional compounds in a boreal forest environment using positive
644 matrix factorization. *Atmospheric Chemistry and Physics* **2016,** *16*, 12715-12731.
645 52. Nieminen, T.; Lehtinen, K. E. J.; Kulmala, M., Sub-10 nm particle growth by vapor
646 condensation-effects of vapor molecule size and particle thermal speed. *Atmospheric Chemistry*
647 *and Physics* **2010,** *10*, 9773-9779.
648 53. Rohrer, F.; Berresheim, H., Strong correlation between levels of tropospheric hydroxyl
649 radicals and solar ultraviolet radiation. *Nature* **2006,** *442*, 184-187.
650 54. Tan, Z.; Lu, K.; Hofzumahaus, A.; Fuchs, H.; Bohn, B.; Holland, F.; Liu, Y.; Rohrer, F.;
651 Shao, M.; Sun, K.; Wu, Y.; Zeng, L.; Zhang, Y.; Zou, Q.; Kiendler-Scharr, A.; Wahner, A.;
652 Zhang, Y., Experimental budgets of OH, HO2 and RO2 radicals and implications for ozone
653 formation in the Pearl River Delta in China 2014. *Atmospheric Chemistry and Physics* **2019,** *19*,
654 7129-7150.
655 55. Kulmala, M.; Dada, L.; Daellenbach, K. R.; Yan, C.; Stolzenburg, D.; Kontkanen, J.;
656 Ezhova, E.; Hakala, S.; Tuovinen, S.; Kokkonen, T. V.; Kurppa, M.; Cai, R.; Zhou, Y.; Yin, R.;
657 Baalbaki, R.; Chan, T.; Chu, B.; Deng, C.; Fu, Y.; Ge, M.; He, H.; Heikkinen, L.; Junninen, H.;
658 Liu, Y.; Lu, Y.; Nie, W.; Rusanen, A.; Vakkari, V.; Wang, Y.; Yang, G.; Yao, L.; Zheng, J.;
659 Kujansuu, J.; Kangasluoma, J.; Petaja, T.; Paasonen, P.; Jarvi, L.; Worsnop, D.; Ding, A.; Liu,
660 Y.; Wang, L.; Jiang, J.; Bianchi, F.; Kerminen, V. M., Is reducing new particle formation a
661 plausible solution to mitigate particulate air pollution in Beijing and other Chinese megacities?
662 *Faraday Discussions* **2021,** *226*, 334-347.
663 56. Riva, M.; Rantala, P.; Krechmer, J. E.; Peräkylä, O.; Zhang, Y.; Heikkinen, L.; Garmash,
664 O.; Yan, C.; Kulmala, M.; Worsnop, D.; Ehn, M., Evaluating the performance of five different
665 chemical ionization techniques for detecting gaseous oxygenated organic species. *Atmospheric*
666 *Measurement Techniques* **2019,** *12*, 2403-2421.
667 57. Ye, Q.; Wang, M.; Hofbauer, V.; Stolzenburg, D.; Chen, D.; Schervish, M.; Vogel, A.;
668 Mauldin, R. L.; Baalbaki, R.; Brilke, S.; Dada, L.; Dias, A.; Duplissy, J.; El Haddad, I.;
669 Finkenzeller, H.; Fischer, L.; He, X.; Kim, C.; Kürten, A.; Lamkaddam, H.; Lee, C. P.;
670 Lehtipalo, K.; Leiminger, M.; Manninen, H. E.; Marten, R.; Mentler, B.; Partoll, E.; Petäjä, T.;
671 Rissanen, M.; Schobesberger, S.; Schuchmann, S.; Simon, M.; Tham, Y. J.; Vazquez-Pufleau,
672 M.; Wagner, A. C.; Wang, Y.; Wu, Y.; Xiao, M.; Baltensperger, U.; Curtius, J.; Flagan, R.;
673 Kirkby, J.; Kulmala, M.; Volkamer, R.; Winkler, P. M.; Worsnop, D.; Donahue, N. M.,

674 Molecular Composition and Volatility of Nucleated Particles from α-Pinene Oxidation between -
675 50 ˚c and +25 ˚c. *Environmental Science and Technology* **2019,** *53*, 12357-12365.
676 58. Olenius, T.; Yli-Juuti, T.; Elm, J.; Kontkanen, J.; Riipinen, I., Chapter 11 - New Particle
677 Formation and Growth: Creating a New Atmospheric Phase Interface. In *Physical Chemistry of*
678 *Gas-Liquid Interfaces*, Faust, J. A.; House, J. E., Eds. Elsevier: 2018; pp 315-352.
679 59. Hallquist, M.; Wenger, J. C.; Baltensperger, U.; Rudich, Y.; Simpson, D.; Claeys, M.;
680 Dommen, J.; Donahue, N. M.; George, C.; Goldstein, A. H.; Hamilton, J. F.; Herrmann, H.;
681 Hoffmann, T.; Iinuma, Y.; Jang, M.; Jenkin, M. E.; Jimenez, J. L.; Kiendler-Scharr, A.;
682 Maenhaut, W.; McFiggans, G.; Mentel, T. F.; Monod, A.; Prevot, A. S. H.; Seinfeld, J. H.;
683 Surratt, J. D.; Szmigielski, R.; Wildt, J., The formation, properties and impact of secondary
684 organic aerosol: current and emerging issues. *Atmospheric Chemistry and Physics* **2009,** *9*, (14),
685 5155-5236.
686 60. Wang, M.; Kong, W.; Marten, R.; He, X. C.; Chen, D.; Pfeifer, J.; Heitto, A.; Kontkanen,
687 J.; Dada, L.; Kurten, A.; Yli-Juuti, T.; Manninen, H. E.; Amanatidis, S.; Amorim, A.; Baalbaki,
688 R.; Baccarini, A.; Bell, D. M.; Bertozzi, B.; Brakling, S.; Brilke, S.; Murillo, L. C.; Chiu, R.;
689 Chu, B.; De Menezes, L. P.; Duplissy, J.; Finkenzeller, H.; Carracedo, L. G.; Granzin, M.;
690 Guida, R.; Hansel, A.; Hofbauer, V.; Krechmer, J.; Lehtipalo, K.; Lamkaddam, H.; Lampimaki,
691 M.; Lee, C. P.; Makhmutov, V.; Marie, G.; Mathot, S.; Mauldin, R. L.; Mentler, B.; Muller, T.;
692 Onnela, A.; Partoll, E.; Petaja, T.; Philippov, M.; Pospisilova, V.; Ranjithkumar, A.; Rissanen,
693 M.; Rorup, B.; Scholz, W.; Shen, J.; Simon, M.; Sipila, M.; Steiner, G.; Stolzenburg, D.; Tham,
694 Y. J.; Tome, A.; Wagner, A. C.; Wang, D. S.; Wang, Y.; Weber, S. K.; Winkler, P. M.; Wlasits,
695 P. J.; Wu, Y.; Xiao, M.; Ye, Q.; Zauner-Wieczorek, M.; Zhou, X.; Volkamer, R.; Riipinen, I.;
696 Dommen, J.; Curtius, J.; Baltensperger, U.; Kulmala, M.; Worsnop, D. R.; Kirkby, J.; Seinfeld, J.
697 H.; El-Haddad, I.; Flagan, R. C.; Donahue, N. M., Rapid growth of new atmospheric particles by
698 nitric acid and ammonia condensation. *Nature* **2020,** *581*, (7807), 184-189.
699 61. Cai, R.; Li, C.; He, X.-C.; Deng, C.; Lu, Y.; Yin, R.; Yan, C.; Wang, L.; Jiang, J.;
700 Kulmala, M.; Kangasluoma, J., Impacts of coagulation on the appearance time method for new
701 particle growth rate evaluation and their corrections. *Atmospheric Chemistry and Physics* **2021,**
702 *21*, (3), 2287-2304.
703 62. Zha, Q.; Yan, C.; Junninen, H.; Riva, M.; Sarnela, N.; Aalto, J.; Quéléver, L.; Schallhart,
704 S.; Dada, L.; Heikkinen, L.; Peräkylä, O.; Zou, J.; Rose, C.; Wang, Y.; Mammarella, I.; Katul,
705 G.; Vesala, T.; Worsnop, D. R.; Kulmala, M.; Petäjä, T.; Bianchi, F.; Ehn, M., Vertical

706 characterization of highly oxygenated molecules (HOMs) below and above a boreal forest
707 canopy. *Atmospheric Chemistry and Physics* 2018, *18*, 17437-17450.
708 63. Kürten, A.; Bergen, A.; Heinritzi, M.; Leiminger, M.; Lorenz, V.; Piel, F.; Simon, M.;
709 Sitals, R.; Wagner, A. C.; Curtius, J., Observation of new particle formation and measurement of
710 sulfuric acid, ammonia, amines and highly oxidized organic molecules at a rural site in central
711 Germany. *Atmospheric Chemistry and Physics* 2016, *16*, 12793-12813.
712 64. Mutzel, A.; Poulain, L.; Berndt, T.; Iinuma, Y.; Rodigast, M.; Böge, O.; Richters, S.;
713 Spindler, G.; Sipilä, M.; Jokinen, T.; Kulmala, M.; Herrmann, H., Highly Oxidized
714 Multifunctional Organic Compounds Observed in Tropospheric Particles: A Field and
715 Laboratory Study. *Environmental Science and Technology* 2015, *49*, 7754-7761.
716 65. Sarnela, N.; Jokinen, T.; Nieminen, T.; Lehtipalo, K.; Junninen, H.; Kangasluoma, J.;
717 Hakala, J.; Taipale, R.; Schobesberger, S.; Sipilä, M.; Larnimaa, K.; Westerholm, H.; Heijari, J.;
718 Kerminen, V. M.; Petäjä, T.; Kulmala, M., Sulphuric acid and aerosol particle production in the
719 vicinity of an oil refinery. *Atmospheric Environment* 2015, *119*, 156-166.

720

721 **Figures.**

722

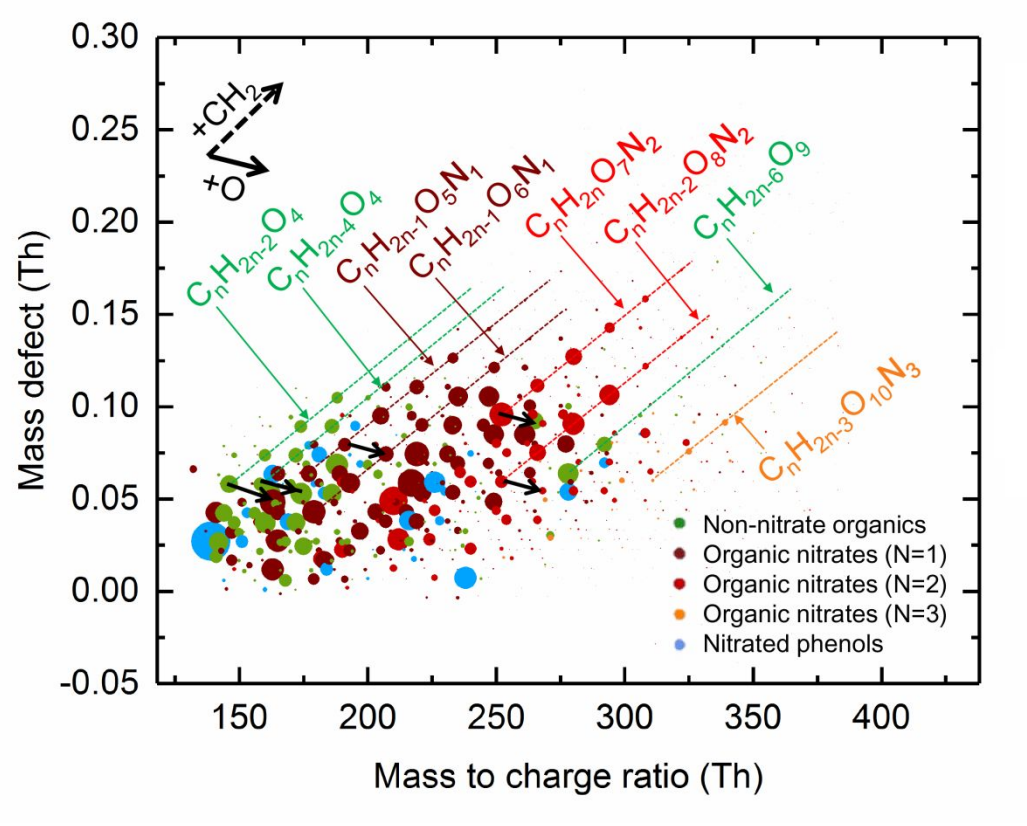

723

724 **Figure 1.** Mass-defect plot of observed oxygenated organic molecules (OOMs) in Beijing of
725 spring. The detected OOMs are marked in the mass-defect plot by their exact mass and mass defect
726 (exact mass subtracted by its unit mass). The differences in molecular composition are shown at
727 regular spacing in the mass-defect plot. Adjacent points on the two direction lines are differed by
728 a -CH_2- group or oxygen atom in composition. The general chemical formulas are annotated by
729 the lines. OOMs with different numbers of nitrogen atoms are shown in different colors. Nitrated
730 phenols are classified separately. The size of the circle corresponds to the concentration of OOMs.

731

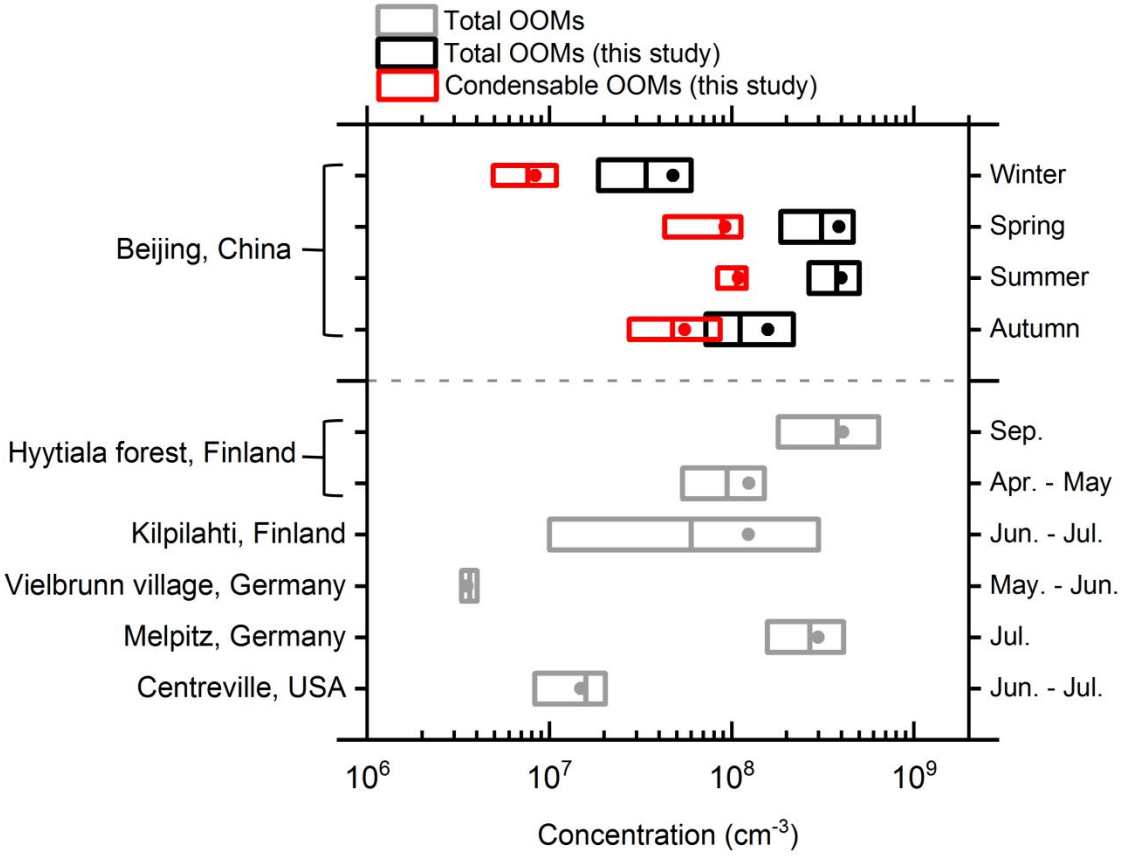

732

733 **Figure 2.** Comparison of atmospheric oxygenated organic molecules (OOMs) measured by nitrate
734 CI-APi-ToF at different locations worldwide. Boxes in black and red are results of total OOMs
735 and condensable OOMs of urban Beijing during the whole observation periods in this study. Boxes
736 in gray are previous results around the world, including Yan et al.[51] and Zha et al.[62] in Hyytiälä
737 forest, Kürten et al.[63] in Vielbrunn village, Mutzel et al.[64] in Kilpilahti, Sarnela et al.[65] in
738 Centreville, and Krechmer et al.[25] in Melpitz. Among them, Vielbrunn and Centreville only report
739 the main oxidation products of monoterpene and isoprene respectively. The boundaries of boxes
740 on x-axis correspond to the 25th and 75th values. Lines and points in boxes are median and mean
741 concentration respectively.

742

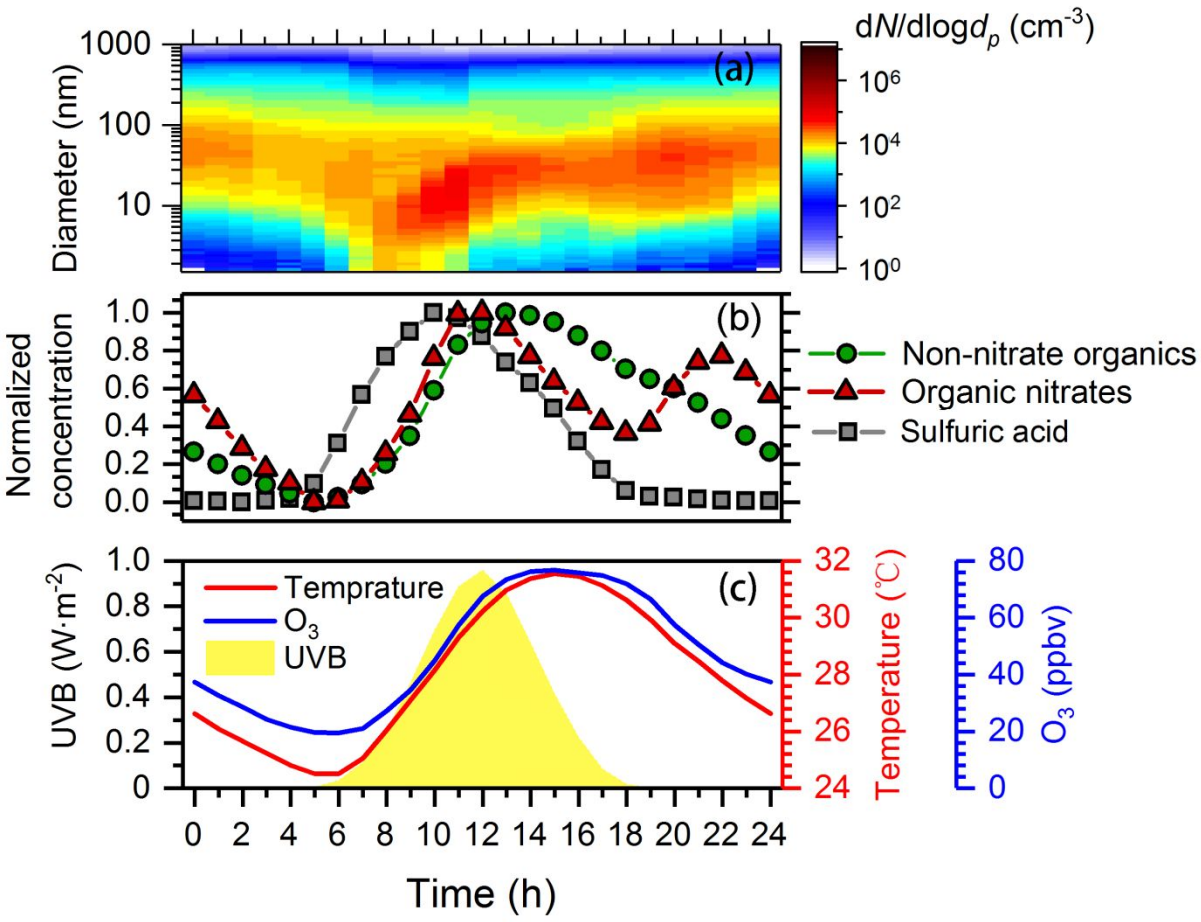

743

744 **Figure 3.** Diurnal variation of observed oxygenated organic compounds and other measured
745 parameters in summer. Note that the particle size distribution shown in the top panel is the
746 averaged result of new particle formation days.

747

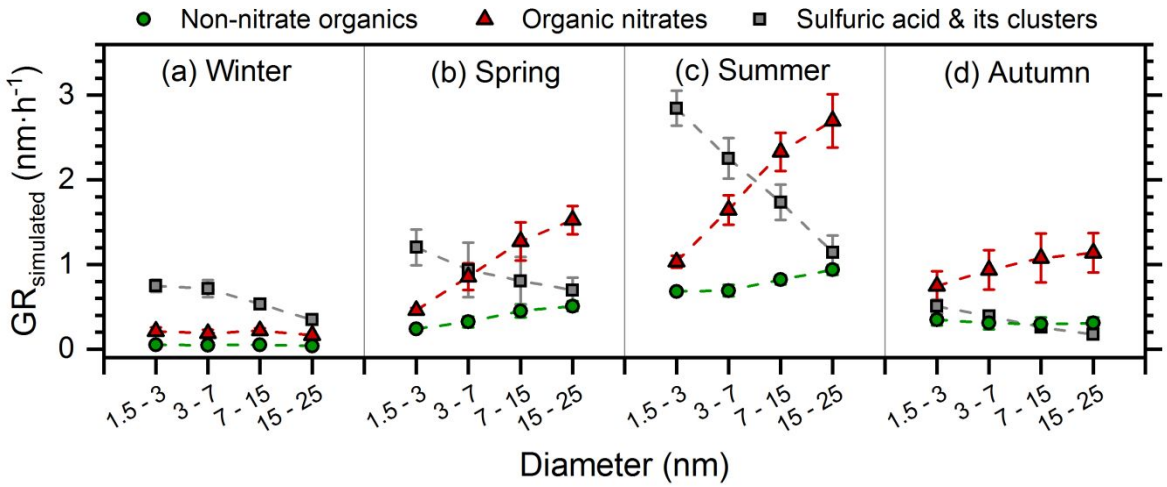

748

749 **Figure 4.** Simulated growth rates contributed by sulfuric acid and its clusters, non-nitrogen OOMs,
750 and nitrogen-containing OOMs. Markers are the averaged results. Error bars are the standard
751 deviations of the simulated results. There are 11, 5, 6 and 5 new particles cases for winter, spring,
752 summer and autumn respectively. The particle growth period of each case (generally 7 am-12 pm)
753 is used for simulation.

754

755

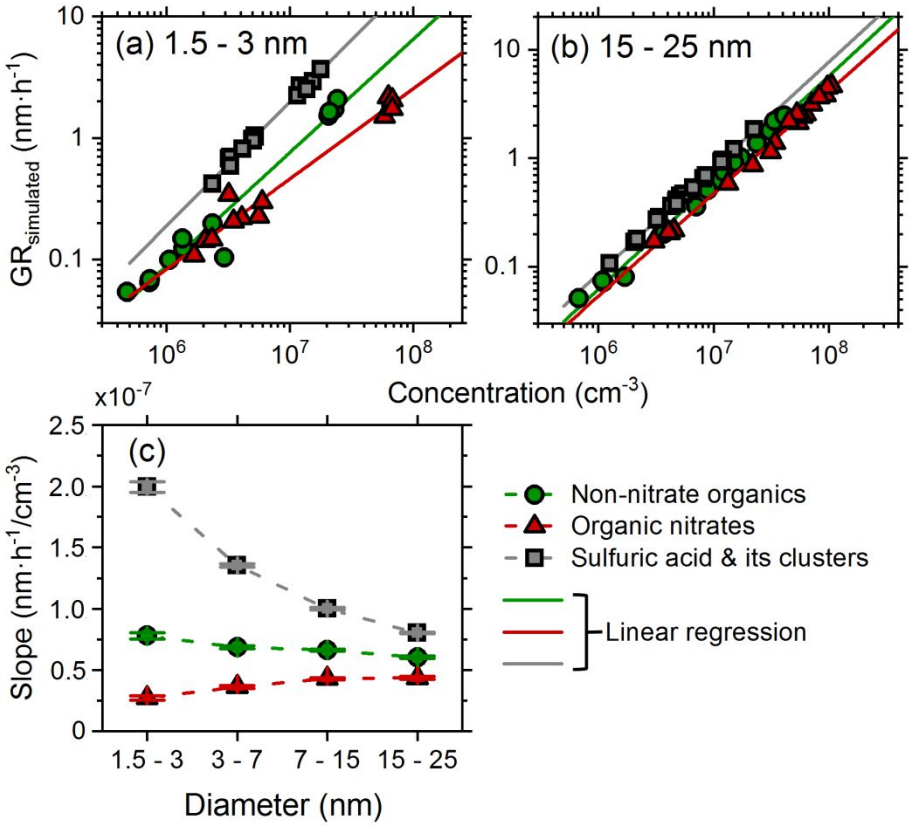

Figure 5. Growth promotion efficiency of different condensing vapors in condensation growth rate. (a)-(b) Vapor concentration and simulated condensation growth rate for different particle size bins, including sulfuric acid and its clusters, non-nitrogen OOMs, and nitrogen-containing OOMs. Solid lines are the linear regressions for different vapors. (c) Slopes of linear regressions ($GR_{simulated}$ v.s. concentration) for different particle size bins, including 1-3 nm, 3-7 nm, 7-15 nm, and 15-25 nm. The green circle represents non-nitrogen OOMs, the red triangle represents nitrogen-containing OOMs, and the gray square represents sulfuric acid and its clusters. The caps of markers in panel (c) are error bars for linear regression uncertainties, which range in 7.2×10^{-10} - 4.3×10^{-9} nm·h^{-1}/cm^{-3}.

769

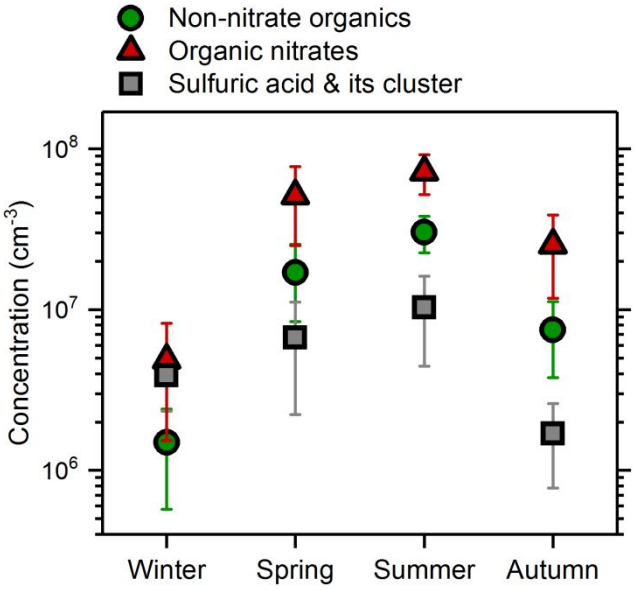

770

771 **Figure 6.** Concentrations of condensable oxygenated organic molecules (OOMs) in four seasons.
772 Markers are the averaged results. Error bars are the standard deviations. The green circle represents
773 non-nitrogen OOMs, the red triangle represents nitrogen-containing OOMs, and the gray square
774 represents sulfuric acid and its clusters.

775

776

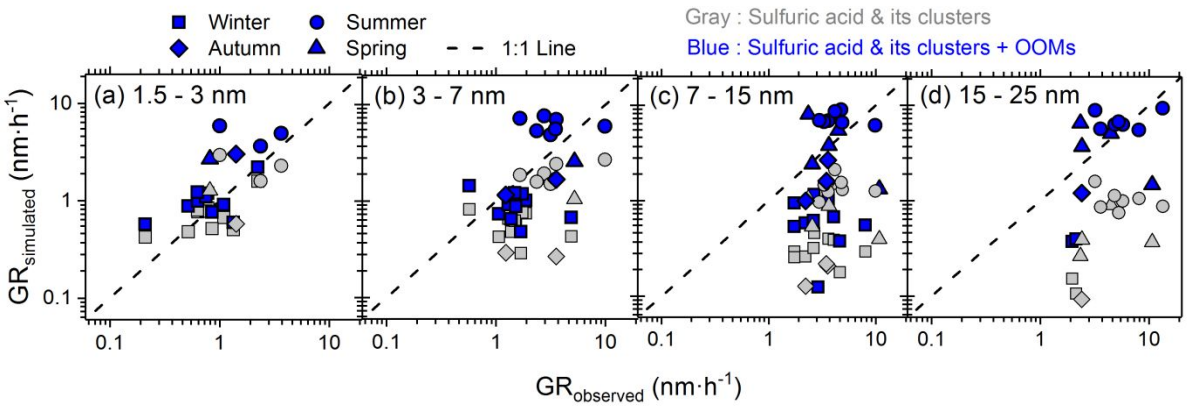

777

778 **Figure 7.** The relations of simulated growth rate and observed growth rate for different particle
779 size bins. Results of different seasons are shown in different shapes of markers. The x-axis is the
780 observed growth rate and the y-axis is the simulated growth rate. The simulated growth rate of
781 sulfuric acid and its clusters are shown in gray, and the blue ones are sulfuric acid and its clusters
782 plus OOMs. The dashed lines are 1:1 lines. Note the observed growth rates are calculated using
783 mode fitting method.